Journal of the European Ceramic Society 7 (1991) 319–327

The Rate-controlling Processes in the Oxidation of HIPped Si_3N_4 with and without Sintering Additives

J. Chen, J. Sjöberg, O. Lindqvist

Department of Inorganic Chemistry, Chalmers University of Technology and University of Göteborg, S-412 96 Göteborg, Sweden

C. O'Meara

Department of Physics, Chalmers University of Technology, S-412 96 Göteborg, Sweden

&

L. Pejryd

Volvo Flygmotor AB, S-461 81 Trollhättan, Sweden

(Received 22 June 1990; revised version received 4 December 1990; accepted 7 December 1990)

Abstract

Various possible rate-controlling processes in the oxidation of HIPped Si_3N_4 with 4 wt% Y_2O_3 and without sintering additives have been studied using TGA, XRD, FTIR, SEM and TEM/STEM methods. It is proposed that, in the temperature range 1000 to 1450°C, the oxidation kinetics of the studied Si_3N_4 materials is mainly determined by O_2 diffusivity in the heterogeneous oxide scales and possibly also by the chemical reactivity of Si_3N_4 materials with O_2. It is shown that the effective O_2 diffusion coefficient in the glassy oxide scales decreases with an increasing volume of devitrified phases and changes with the structural form of the oxide scales. This may explain why experimental oxidation kinetic curves usually deviate from the conventional parabolic growth law.

Die bei der Oxidation von heißisostatisch gepreßtem Si_3N_4 mit 4 Gew.% Y_2O_3 bzw. ohne Sinteradditive möglichen diskreten geschwindigkeitsbestimmenden Mechanismen wurden mittels TGA, XRD, FTIR, SEM und TEM/STEM untersucht. Im Temperaturbereich von 1000°C bis 1450°C wird die Oxidationskinetik der untersuchten Si_3N_4-Materialien hauptsächlich durch die O_2-Diffusion in den heterogenen Oxidschichten und wahrscheinlich auch durch die chemische Reaktion von Si_3N_4 mit O_2 bestimmt. Der effektive O_2-Diffusionskoeffizient in den glasigen Oxidschichten nimmt mit zunehmendem Anteil an auskristallisierten Phasen ab und ändert sich mit dem Aufbau der Oxidschichten. Dies könnte erklären, warum die experimentell bestimmte Oxidationskinetik im allgemeinen vom konventionellen parabolischen Zeitgesetz abweicht.

On a étudié par TGA, XRD, FTIR, SEM et TEM/STEM, les différents mécanismes pouvant contrôler la cinétique d'oxydation du Si_3N_4 élaboré par pressage isostatique à chaud, additionné de 4% massiques de Y_2O_3 ou sans adjuvants. On considère que, dans une gamme de températures allant de 1000 à 1450°C, la cinétique d'oxydation des matériaux Si_3N_4 étudiés est principalement déterminée par la diffusivité de O_2 dans les couches hétérogènes d'oxydes et probablement également par la réactivité chimique du Si_3N_4 avec O_2. On montre que le coefficient de diffusion effectif de O_2 dans les couches vitreuses d'oxyde diminue avec le volume des phases vitrifiées et change avec la formule des couches d'oxydes. Cela peut expliquer la raison pour laquelle les courbes expérimentales de cinétique d'oxydation s'écartent habituellement de la loi de croissance parabolique classique.

1 Introduction

Oxidation of Si_3N_4 materials is considered to be one of the causes of material degradation in the

Journal of the European Ceramic Society 0955-2219/91/$3.50 © 1991 Elsevier Science Publishers Ltd, England. Printed in Great Britain

application of these materials in highly oxidizing combustion environments such as in heat engines. The oxidation of pure Si_3N_4 at high oxygen potentials can be expressed by

$$Si_3N_{4(s)} + 3O_{2(g)} = 3SiO_{2(s)} + 2N_{2(g)} \quad (1)$$

However, the oxidation of Si_3N_4 materials sintered with the use of sintering additives is more complex. During oxidation, the amorphous oxide scales which form on the materials tend to devitrify. For some Si_3N_4 materials, the additive metal cations have been found to concentrate in the oxide scales.[1-3] Dissolution of Si_3N_4 materials in the glassy oxide scales may also occur, depending on the nature of the amount of the sintering additives used and on the oxidation conditions.

The relationships between the oxidation weight gain (w) or thickness (L) of the oxide scales and the oxidation time (t) and the temperature (T) have been described by the following equations:

$$L^2 \text{ (or } w^2) = kt \quad (2)$$

and

$$k = k_0 \exp\left(-\frac{E_a}{RT}\right) \quad (3)$$

where k_0 is the pre-exponential factor and R the gas constant. An activation energy (E_a), which has quite often been used to interpret the oxidation process, can be deduced from eqn (3) by assuming that k_0 is independent of time and temperature. It has been noted that the above parabolic equation does not fit well many of the reported weight gain versus time curves, as the oxidation rate usually decreases faster with time than predicted. This is especially true in long-term oxidation tests.[4-6] Furthermore, the deduced E_a values are higher than those corresponding to O_2 diffusion in amorphous silica. Not only do they vary considerably from one material to another,[3,7,8] but they also increase with increasing temperature for the same material.[1,3,9] For some Si_3N_4 materials, it has been suggested[3,10] that during oxidation the outward diffusion of additive metal cations from grain boundaries to the oxide scales may be the rate-controlling process. However, some oxidation work[6,11] has shown that in a certain temperature range the weight gain decreases with increasing temperature. From these experimental results negative activation energies may be formally deduced and it is therefore impossible to explain the oxidation process on the basis of the activation energies obtained.

The reoxidation work by Cubicciotti & Lau[2,3] has shown that for MgO-containing Si_3N_4 (NC 132) the oxide scale is non-protective, while for the Y_2O_3-doped Si_3N_4 (NC X34) the scale has a degree of protectiveness. Few investigations have been carried out on the oxidation behaviour of the HIPped Si_3N_4 with minor amounts of Y_2O_3 as sintering additive or without sintering additives. The oxidation behaviour of such materials can be expected to differ considerably from that of MgO-containing Si_3N_4 materials and of the materials doped with large amounts of Y_2O_3, because of the expected different properties of both the grain boundary phases and the oxide scale.

The purpose of the present work has been to investigate the rate-controlling processes in the oxidation of the HIPped Si_3N_4 with 4 wt% Y_2O_3 as sintering additive and to find a relevant theoretical description of the process. A HIPped Si_3N_4 without sintering additive has been chosen as reference.

2 Experimental

2.1 Materials

One Si_3N_4 material HIPped with 4 wt% Y_2O_3 (denoted 4YSN) and one without sintering additives (denoted 0YSN) were used in this study. The former was produced from UBE E10 and E03 Si_3N_4 powders, and the latter from UBE E10 powder. The densities of both materials exceed 99% of the theoretical density.

2.2 Microstructural analysis

The microstructures of the as-received and oxidized materials were characterized by a combination of X-ray diffractometry (XRD) and analytical transmission electron microscopy (STEM/EDX) using a Jeol 200 FX instrument equipped with a Link Systems AN 10000 EDX spectrometer. Following oxidation, characterization of the oxide scales of 4YSN and 0YSN was carried out on surface and cross-section by scanning electron microscopy (SEM) using a Cam Scan S-4 80 DV instrument equipped with a Link EXL System.

2.3 Oxidation experiments

Specimens for oxidation were cut with a diamond saw into square samples ($\approx 1 \times 1 \times 0{\cdot}3$ cm), polished with SiC paper and with various grades of diamond spray, and then ultrasonically cleaned in acetone and in alcohol. Sample holders of the same Si_3N_4 materials were used. The samples were oxidized in an alumina tube furnace in the temperature range 1000 to 1450°C in flowing dry air with 10 litres/h flow rate. The samples were intermittently taken out from the furnace and weighed on an analytical balance with

$\pm 0{\cdot}015$ mg sensitivity. The absolute errors in weighing caused by humidity and other factors were within $\pm 0{\cdot}050$ mg.

In order to investigate the effects on the oxidation rate of possible crystallization of the grain boundary glassy phase during the oxidation period, pre-oxidation treatment of 4YSN was performed. To enhance the nucleation and growth processes, the 4YSN samples were heated progressively through 1000, 1100, 1200 and 1300°C in static air for 1000 min at each temperature. Following this, about 200 μm of the exposed sample surfaces was ground away in order to remove any reacted or affected surface zone caused by oxidation or by possible yttrium concentration depletion. The samples were then polished and cleaned as described above. The pre-treated samples (denoted PTSN) were then re-oxidized at 1250 or 1450°C for 100 h. It was though that the Y^{3+} diffusion process in the second oxidation period would be hindered by the expected crystallization[12] of the glassy grain boundary phase occurring in the first pre-oxidation treatment. Therefore, if the Y^{3+} diffusion plays an important role during oxidation, the measured oxidation rate of the pre-oxidized 4YSN should be lower than that of the as-received 4YSN.

2.4 Characterization of the oxide scales by FTIR

Fourier transform infrared transmission spectroscopy (FT-IRTS) analysis was used to investigate the structure of glassy oxide scales. Specimens of 4YSN were crushed in a steel vibrating mill. The powder obtained was cleaned in boiling 0·1M HCl and subsequently in deionized water to remove any Fe and Cl introduced during crushing. The powder was oxidized in the temperature range 1000 to 1400°C in dry air with 10 litres/h flow rate. Pellets (the weight ratio of KBr to powder sample was 150 mg:0·6 mg) were made for FT-IRTS measurements.

3 Results

3.1 Microstructures of the as-sintered materials

The microstructure of the 4YSN was found to consist of a major β-Si_3N_4 phase and a small volume of secondary crystalline phase. Combined X-ray and electron diffraction indicated the secondary crystalline phase to be $Y_2Si_2O_7$. A wide grain size distribution (0·1–10 μm) was observed for the β-Si_3N_4 phase and the sub-micron grains were associated with multigrain pockets of $Y_2Si_2O_7$ (Fig. 1). Centred dark field imaging in the TEM showed the presence of thin amorphous films (1–4 nm) between the grains in the microstructure (Fig. 2). 0YSN was found to consist of sub-micron β-Si_3N_4 grains (Fig. 3) separated by thin intergranular amorphous films and small glassy pockets at triple grain junctions (Fig. 4).

3.2 Weight gain versus time curves of 4YSN, 0YSN and PTSN

The oxidation time dependence of the weight change of 4YSN, 0YSN and PTSN in the temperature range 1000 to 1450°C is shown in Figs 5 and 6. For 4YSN

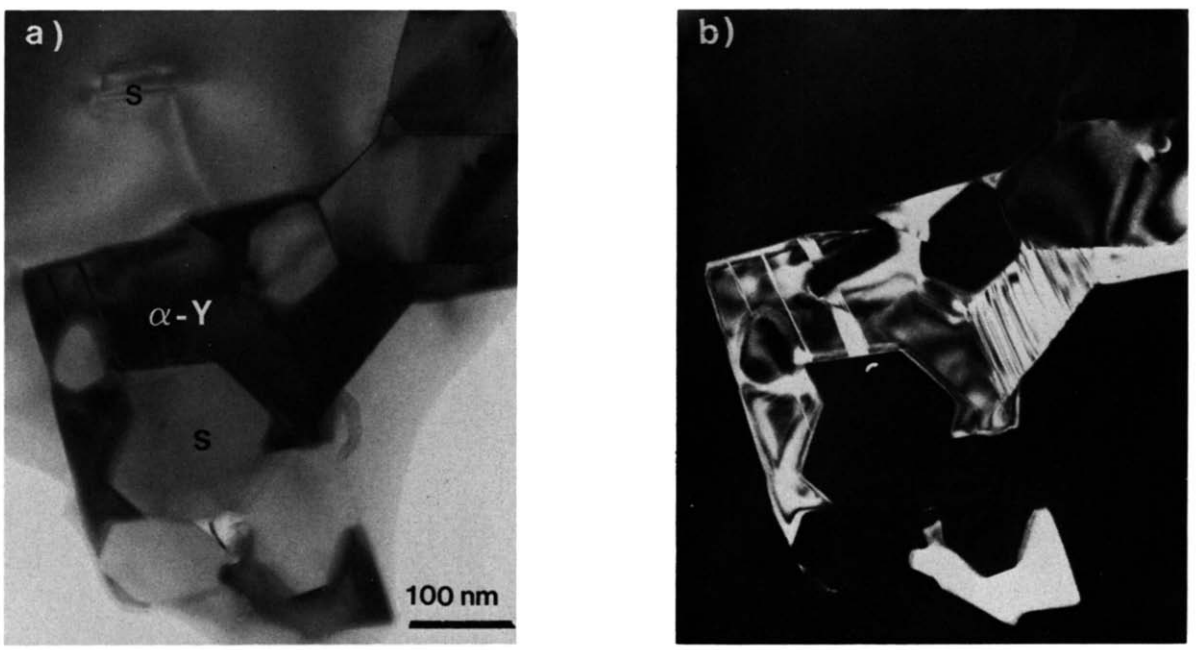

Fig. 1. TEM micrographs showing the general microstructure of 4YSN: (a) Bright field image showing a multigrain $Y_2Si_2O_7$ region (Y) containing submicron β-Si_3N_4 grains (S); (b) Dark field image using a $Y_2Si_2O_7$ diffracted beam.

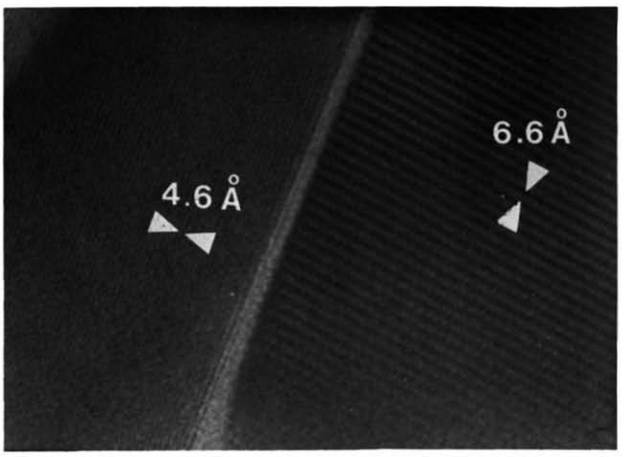

Fig. 2. Lattice fringe TEM image showing the presence of a thin amorphous film (1–3 μm) between β-Si_3N_4 grains and $Y_2Si_2O_7$ grains in 4YSN. The lattice fringes correspond to the (100) planes in the $Y_2Si_2O_7$ grains (spacing 4·6 Å) and the (100) planes in the β-Si_3N_4 grains (spacing 6·6 Å).

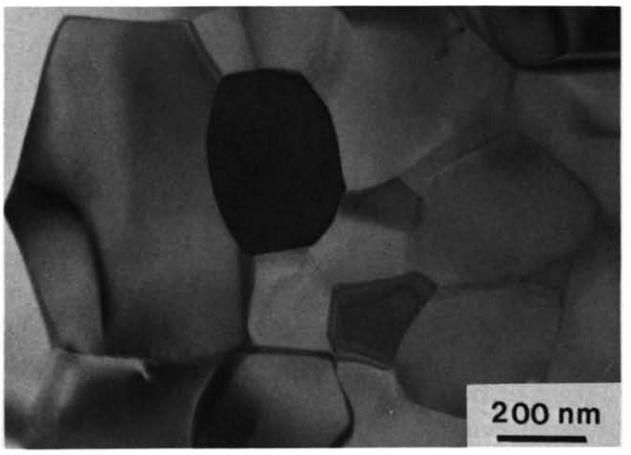

Fig. 3. TEM micrograph showing the sub-micron β-Si_3N_4 grain size distribution of 0YSN.

the weight gain decreased with increasing temperature from 1000 to 1350°C and increased considerably at 1450°C. The rate of weight gain at each temperature decreased with increasing time, and there was little weight change during 20–80 h exposure period. After a longer oxidation period, especially at the higher temperature (1450°C), however, the rate increased considerably again.

For 0YSN, the weight gain at 1000°C was nearly identical to that of 4YSN. A similar decrease in weight gain with increasing temperature up to 1450°C was also observed. The weight gain of 0YSN at 1450°C was lower than that of 4YSN during the initial 50 h, but the difference then gradually decreased after the longer oxidation period.

For PTSN, the weight gain was similar to that of 4YSN at 1250°C and at 1450°C for the first 20 h. The weight gain was slightly higher than that of 4YSN at 1450°C after a longer oxidation period.

3.3 XRD of the oxidized 4YSN, 0YSN and PTSN

XRD analysis revealed that after oxidation the crystalline phases formed in the scales of 0YSN were α-cristobalite and some Si_2N_2O, while for 4YSN α-cristobalite and yttrium disilicates were found. N-Apatite phase was observed at 1000°C but was not found at higher temperatures. A slightly broadened diffraction line at $d = 4{\cdot}07$ Å (of α-cristobalite) can be seen in the XRD patterns, which indicates the existence of amorphous or microcrystalline silica phase. A more extensive XRD study has confirmed that this diffraction line started to appear after oxidation at 1000°C for a short period (< 2h), and its relative intensity was enhanced with increasing oxidation time and temperature. No phase change in the bulk 4YSN samples could be detected after the pre-oxidation treatment. This may be due to the small amount of the crystalline grain boundary phases, as observed in TEM, whose changes, if any, may be far below the detection limit of the diffractometer. No attempt, therefore, was made to

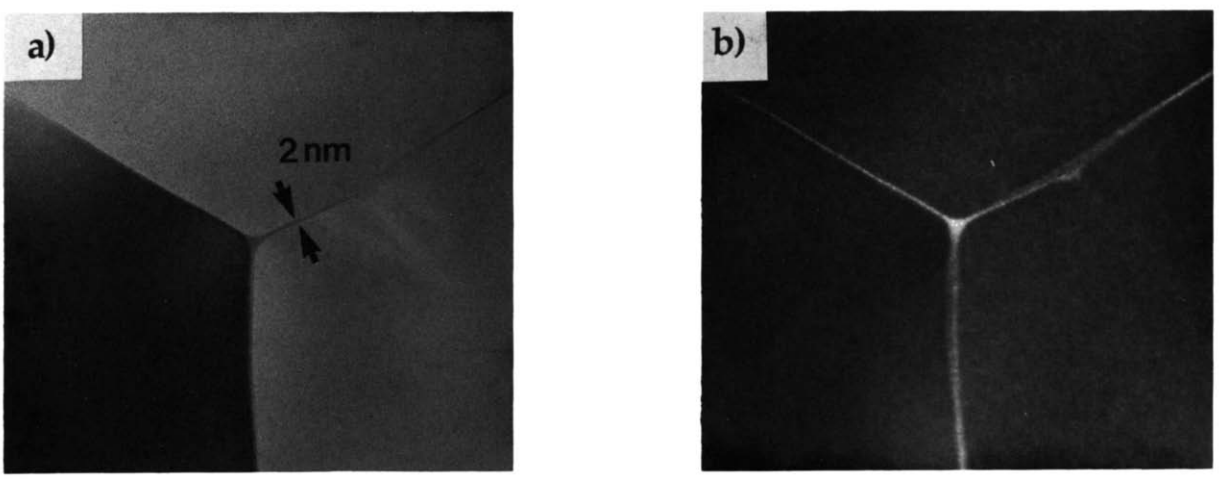

Fig. 4. TEM micrograph of 0YSN: (a) Bright field image; (b) centred dark field image showing the presence of a thin amorphous film which surrounds the β-Si_3N_4 grains and a small glassy pocket at a triple grain junction.

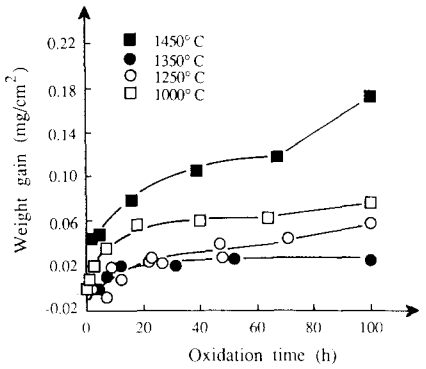

Fig. 5. Oxidation time dependence of weight gain of 4YSN at various temperatures.

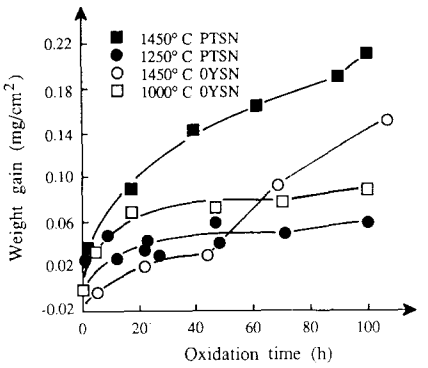

Fig. 6. Oxidation time dependence of weight gain of 0YSN, PTSN at various temperatures.

further investigate the effect of the crystallinity of grain boundary glassy phase on the oxidation behaviour.

3.4 Microstructures of oxidized 4YSN and 0YSN

TEM examination of the sub-scalar region of 4YSN following oxidation at 1000, 1250, 1350 and 1450°C did not indicate any significant change in the microstructure compared to that of the as-received material. SEM examination in secondary electron (SE) and backscattered electron (BE) mode was carried out on surface and cross-sections of oxidized 4YSN material. The oxide scales were seen to be cracked at all temperatures (Fig. 7). Using SEM in BE mode the $Y_2Si_2O_7$ detected in the scale by XRD could be identified by atomic number contrast combined with EDX analysis. The $Y_2Si_2O_7$ phase was observed to have a distinct morphology at each temperature examined. As can be seen in Fig. 7, at 1000°C the intergranular morphology and distribution of the $Y_2Si_2O_7$ in the bulk material was preserved in the scale. At 1250 and 1350°C, the morphology of the $Y_2Si_2O_7$ phase was observed to have become more particulate and a few large crystals of $Y_2Si_2O_7$ were detected. At 1450°C a high density of large $Y_2Si_2O_7$ crystals was observed. In transverse section the $Y_2Si_2O_7$ phase was found to occur through the depth of the oxide scales, while

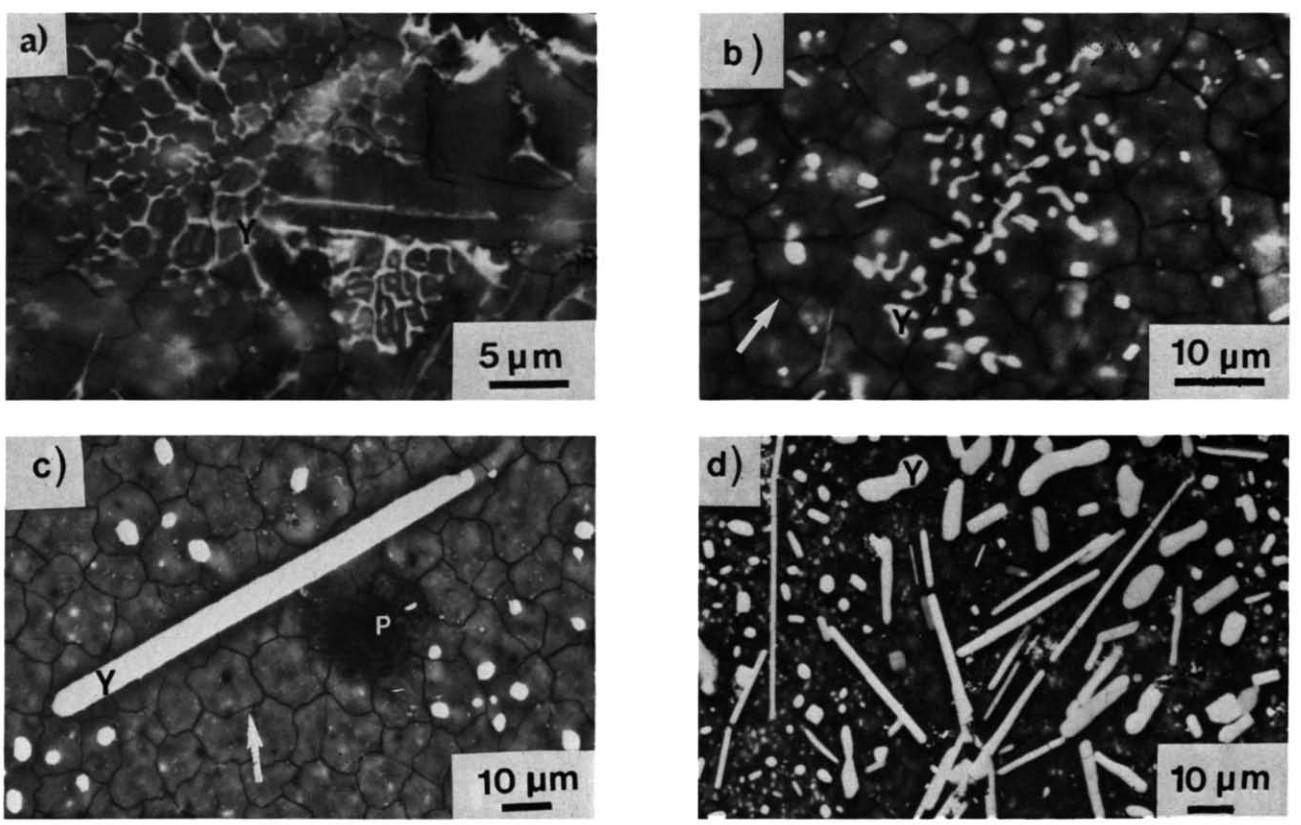

Fig. 7. SEM backscattered images of the oxidized surfaces of 4YSN showing $Y_2Si_2O_7$ grains (Y) and cracks in the oxide scales after oxidation for 100 h at (a) 1000°C; (b) 1250°C; (c) 1350°C; and (d) 1450°C.

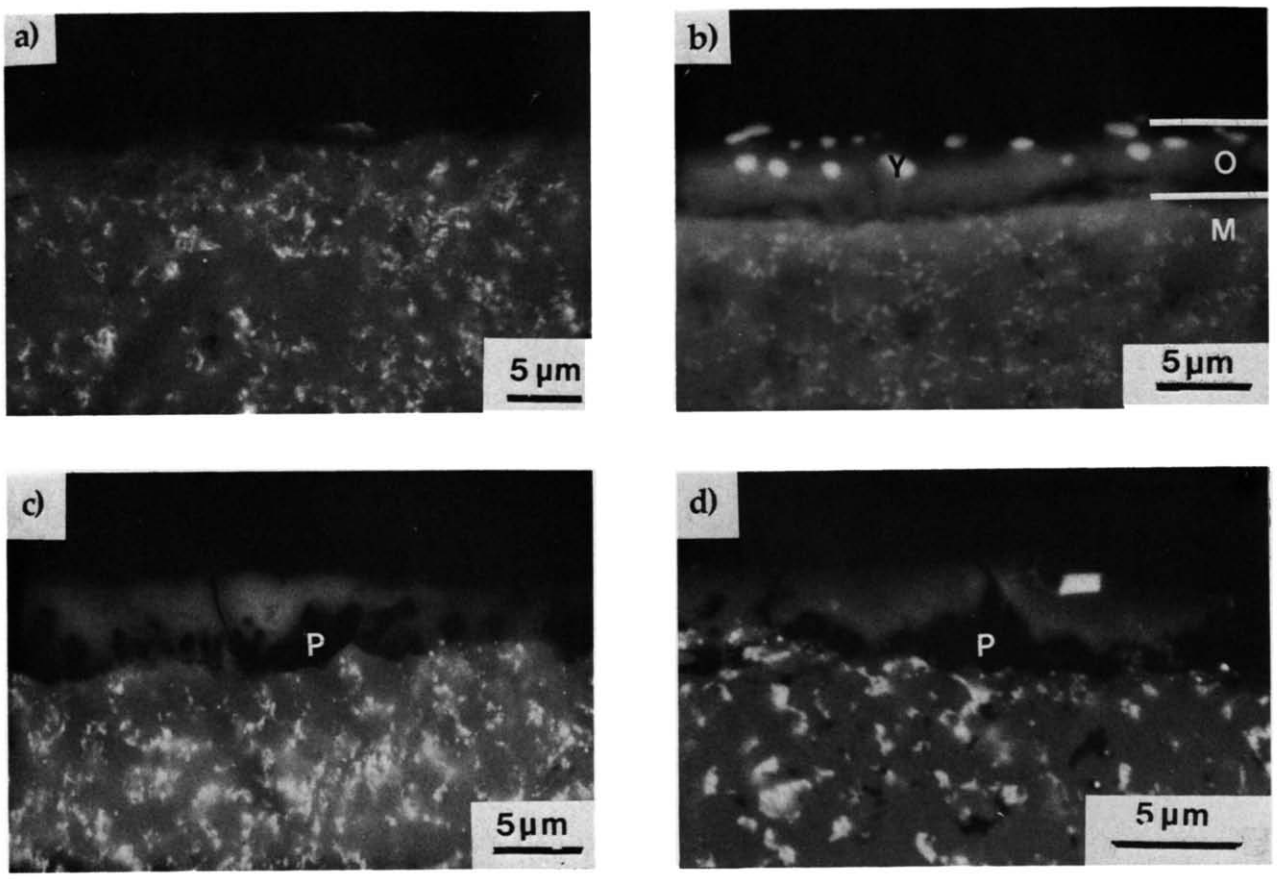

Fig. 8. SEM backscattered images of cross-sections of the oxide scales (O) and the underlying bulk 4YSN (M) after oxidation for 100 h at (a) 1000°C; (b) 1250°C; (c) 1350°C; and (d) 1450°C. Gas pores (P) can be seen at the bottom of the oxide scales.

EDX analysis through the oxide scale to a distance of ~5 mm into the matrix indicated that there was no yttrium concentration depletion in the matrix below the oxide scale. Small pores, which were visible at the bottom of the oxide scales, had developed into interconnecting structure at higher temperatures (Fig. 8).

3.5 FT-IRTS of 4YSN powder after exposure

Comparison of present transmission spectra and reflectance spectra[13] obtained from oxidized surfaces of the Si_3N_4 specimens showed essentially the same spectral features. As can be seen in the infrared spectra (Fig. 9), for oxidation at 1250 and 1400°C, considerable splitting and broadening of the bands between 350 cm^{-1} and 1300 cm^{-1} clearly indicate the formation of SiO_2 (at 493, 620, 797, 1100 cm^{-1}) and $Y_2Si_2O_7$ (e.g. at ~1040 cm^{-1}). It is interesting to note that oxidation at 1000°C for 20 h only led to a slightly broadened band at ~1100 cm^{-1} and produced some weak bands at e.g. ~500 cm^{-1}, even though the measured weight gain at 1000°C was higher than that for the sample oxidized at 1250°C. This suggests that those relatively sharp bands of silica may be assigned to SiO_2 with an ordered structure or to cristobalite. Together with the XRD

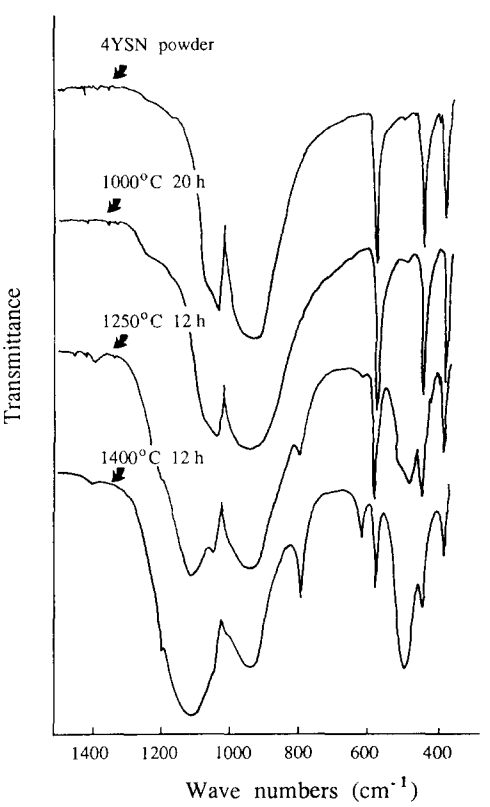

Fig. 9. FTIR spectra of oxidized 4YSN powder at various temperatures.

results, this phenomenon suggests that silica formed at the initial stage of oxidation in the low temperature range may be primarily amorphous or microcrystalline, which is similar to the observations in the oxidation of some sintered Si_3N_4 materials[10] and CVD Si_3N_4.[14] More extensive work is to be carried out in order to better evaluate the spectra obtained by this technique.

4 Discussion

The oxidation rates of the materials examined in this work decrease with increasing exposure time, indicating that the oxidation is a diffusion-controlled process. The most striking features of the oxidation kinetics of 4YSN are that (a) the weight gain decreases with increasing temperature from 1000 to 1350 °C; (b) oxidation undergoes a long near-zero rate period in the temperature range 1000 to 1350 °C and (c) after a longer oxidation period the oxidation rate increases again. It is obvious that the oxidation kinetics cannot be described by eqns (2) and (3).

Since it was observed that 4YSN showed rather similar oxidation kinetics to those of 0YSN and there was not any significant effect of the pre-oxidation treatment on the oxidation rate, for 4YSN the influence on the oxidation kinetics of the possible changes in internal grain boundary phase (i.e. crystallization and/or Y^{3+} migration) from the grain boundaries to the oxide scales does not appear to be significant. In the following paragraphs, therefore, O_2 diffusion in the oxide scales and the factors which could affect this process are discussed.

In order to describe the O_2 diffusion process during oxidation of Si, Deal & Grove[15] deduced a theoretical expression which accounts for both O_2 diffusivity in the formed silica and the chemical reactivity of Si with O_2. The simplified equation has the form:

$$L = \frac{A}{2}\left(\sqrt{1 + \frac{4B}{A^2}t} - 1\right) \tag{4}$$

where $A = 2D/K_c$, $B = 2DC^*/N_1$, L is the thickness of the oxide scale; D is the diffusion coefficient of O_2 in the oxide scale (here the small contribution from the O^{2-} diffusion is ignored); K_c is the first-order reaction constant ($Si + O_2 = SiO_2$) at the SiO_2/Si interface; N_1 is the number of O_2 needed to form a unit volume of oxide; C^* is the limit solubility of O_2 in the oxide. Because of the remarkable similarity in the description of O_2 diffusion in the SiO_2 surface layer formed during the oxidation of Si and Si_3N_4

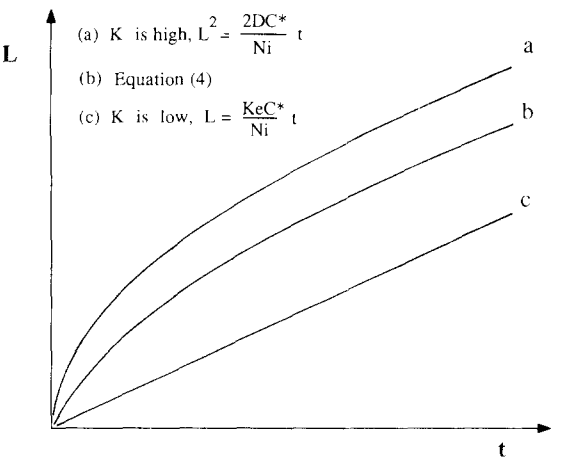

Fig. 10. The shifts of L–t curves with decreasing K_c indicating the possible role of the chemical reactivity of Si_3N_4 materials with O_2 in controlling the oxidation kinetics. (a) O_2 diffusion-controlled process; (b) O_2 diffusion and chemical reaction controlled processes; and (c) chemical reaction controlled process.

materials, the Deal & Grove equation is used to describe the oxidation kinetics of the Si_3N_4 materials in present paper. K_c is therefore the first-order reaction constant for the chemical reaction (1).

According to eqn (4), the oxidation kinetics of the Si_3N_4 materials is mainly determined by K_c, C^* and D. Figure 10 shows that with a decrease of K_c the oxidation kinetics could be altered from an O_2 diffusion controlled process to a chemical reaction controlled process. Because of the highly covalent bonding structure of Si_3N_4 compound, the chemical reaction between Si_3N_4 and O_2 may not be as easy a process as that between Si and O_2. The K_c value for Si_3N_4 materials may be very small. It is therefore reasonable to assume that K_c plays a role in affecting the oxidation processes. C^* may depend on the nature of the oxide scale, but as it has been confirmed to be independent of O_2 partial pressure within a broad range,[16] the oxidation rate would therefore be largely unaffected by the O_2 partial pressure, as confirmed by other experiments.[3,10] D depends not only on temperature and the chemical composition of the oxide scale, but, as illustrated later, it also depends on the relative amount of devitrified phases in the amorphous oxide scale and on the structural form of the oxide scale.

Normally, D increases exponentially with temperature in amorphous silica, which may lead to a considerable increase in the oxidation rate. Contrary to this suggestion, the present experimental results show that the weight gain decreases with increasing temperature from 1000 to 1350 °C. This can be explained if one takes into account the effect of devitrification of the amorphous oxide scales on the O_2 diffusion coefficient during the oxidation period.

Present XRD and FT-IRTS studies have confirmed that within the studied temperature region, the higher the temperature or the longer the oxidation time, the more pronounced the devitrification of the oxide scales will be. This, according to the calculations using the formula given in Ref. 17 would result in a considerable decrease in the effective O_2 diffusion coefficient (D_e). The calculations have shown that the magnitude of the decrease in D_e is also determined by the structural form of the oxide scale. For instance, if the oxide scale contains 20 vol.% devitrified phases which are randomly dispersed in the amorphous phase, $D_e/D_a \sim 75\%$ (assume $D_a/D_c > 10$, D_a and D_c represent the O_2 diffusion coefficients in the amorphous phase and in the crystalline phases, respectively); if, on the other hand, the devitrified phases form lamina in the amorphous oxide scale, D_e will decrease to D_c. It is clear that D in eqn (4) should be considered to decrease with time, and the oxidation rate will therefore decrease faster with time, as observed in the present studies and in the literature.[4-6] If the oxide scale develops to form a laminated structure during oxidation, the oxidation rate can be extremely low. Because devitrification of the amorphous oxide scales is more pronounced at higher temperature, the weight gain will decrease with increasing temperature, provided that the decrease in the D value due to the devitrification effect is larger than the increase in the D value due to higher O_2 mobility at the higher temperature. Present kinetic curves in the temperature range 1000 to 1350°C and other similar results[6] are consistent with this suggestion.

The role of N_2 formed during oxidation in influencing the oxidation rate has not as yet been clarified. Nitrogen may be released from the oxide scales either by bubble-floating or by outward N_2 or N^{3-} diffusion through the oxide scales. Using Stokes' equation, it can be calculated that the rising speed of N_2 bubbles in vitreous silica is extremely slow (at 1450°C, it is about $6{\cdot}6 \times 10^{-7}$ μm/h for a bubble with 1 μm radius). Hence, it is believed that the N_2 formed in the oxide scale would not escape from the oxide scales in this way. This is also in agreement with the SEM observation that few bubble-like pores were seen on the surface of the oxide scales. N_2 diffusion through the oxide scales is a possible way of releasing N_2 during oxidation, as its diffusion coefficient in fused silica is close to that of O_2.[16] The counter-diffusion of O_2 and N_2 has been considered by Schlichting[18] to be responsible for the lower oxidation rates of Si_3N_4 materials, but it is argued that this nitrogen blocking effect should be small due to the fact that there is lack of dependence of the oxidation kinetics on the ambient nitrogen partial pressure.[19]

As seen in Figs 5 and 6, the oxidation rate dramatically increased again after a longer oxidation period (>60 h), especially at 1450°C. The explanation for this phenomenon (S-shape curves) may be found in a change in the nature of the oxide scales. During the oxidation experiments, in order to measure the weight changes, the oxidized samples were frequently taken out of the furnace, quickly cooled to the room temperature and put back into the furnace. These procedures may to some extent have damaged the integrity of the oxide scales, in addition to the damage caused by thermal mismatch of oxide and nitride and by the large volume change in the phase transformation of $\alpha \Leftrightarrow \beta$ cristobalite. Since the cracks probably exist during the whole exposure period, they would not be the only reason responsible for the S-shape curves. The possible cause may be the buildup of interconnected N_2 pores at the oxide/nitride interfaces during the long exposure period, as O_2 molecules could easily flow through the cracks into the interconnected N_2 pores and cause rapid re-oxidation. The observed S-shape curves call for further investigation under the long-term and cyclic oxidation conditions.

In the present work, the oxidation behaviour of Si_3N_4 materials with and without minor amounts of Y_2O_3 as sintering additive has strongly suggested the important role of O_2 diffusion in controlling the oxidation kinetics. Since the nature of the oxide scale formed during oxidation of Si_3N_4 materials may be changed depending on oxidation temperature and duration as well as materials themselves, further work is considered to be necessary to achieve a better understanding of how the chemical compositions, microstructures and closely related O_2 diffusivity could affect the oxidation or hot corrosion behaviour of these or other Si_3N_4-based materials.

5 Conclusions

The oxidation studies on HIPped Si_3N_4 material with 4wt% Y_2O_3 as sintering additive have shown that the influence on the oxidation kinetics of the possible changes in internal grain boundary phase (i.e. crystallization and/or Y^{3+} migration) from the grain boundaries to the oxide scales does not appear to be significant. For the temperature range examined, the oxidation kinetics appears to be mainly determined by O_2 diffusivity in the heterogeneous oxide scales and possibly also by the

chemical reactivity of Si_3N_4 materials with O_2. The effective O_2 diffusion coefficient in the oxide scale decreases with an increasing amount of devitrified phases and also changes with the structural form of the oxide scale.

Acknowledgements

The authors thank Dr R. Pompe for his valuable discussions. Financial support from the Swedish Board for Technical Development is gratefully acknowledged.

References

1. Tripp, W. C. & Graham, H. C., Oxidation of Si_3N_4 in the range 1300°C to 1500°C. *J. Am. Ceram. Soc.*, **59**(9–10) (1976) 399–403.
2. Cubicciotti, D. & Lau, K. H., Kinetics of oxidation of hot-pressed silicon nitride containing magnesia. *J. Am. Ceram. Soc.*, **61**(11–12) (1977) 512–17.
3. Cubicciotti, D. & Lau, K. H., Kinetics of oxidation of yttria hot-pressed silicon nitride. *J. Electrochem. Soc.*, **126**(10) (1979) 1723–8.
4. Nassif, N. & Hanna, S. B., High-temperature corrosion of reaction-sintered silicon nitride. *Thermochim. Acta*, **79** (1984) 305–14.
5. Hanna, S. B., Grathwohl, G. & Thümmler, F., Oxidation behaviour of hot-pressed silicon nitride containing minor amounts of magnesia. *Keram. Z.*, **36**(3) (1984) 132–4.
6. Knoch, H. & Schlichting, J., Oxidation behaviour of Y_2O_3-containing hot-pressed silicon nitride. *Sprechsaal*, **114**(2) (1981) 99–103.
7. Hanna, S. B., Abou Sekkina, M. M. & Rashad, M., Kinetics of the thermal behaviour of hot-pressed silicon nitride in the temperature range 1250 to 1400°C. *Thermochim. Acta*, **77**(1–3) (1984) 191–200.
8. Sato, T., Haryu, K., Endo, T. & Shimada, M., High-temperature oxidation of silicon nitride-based ceramics by water vapour. *J. Mater. Sci.*, **22** (1987) 2635–40.
9. Babini, G. N., Bellosi, A. & Vincenzini, P., Oxidation of silicon nitride hot-pressed with Y_2O_3 + MgO. *J. Mater. Sci.*, **18**(1) (1983) 231–44.
10. Singhal, S. C., Thermodynamics and kinetics of oxidation of hot-pressed silicon nitride. *J. Mater. Sci.*, **11** (1976) 500–9.
11. Patel, J. K. & Thompson, D. P., The low-temperature oxidation problem in yttria-densified silicon nitride ceramics. *Brit. Ceram. Trans. J.*, **87** (1988) 70–3.
12. Pejryd, L., Heat-treatment of HIPed Si_3N_4 ceramics. *J. Hard Mater.*, **1**(2) (1990) 137–43.
13. Hench, L. L. & Freiman, S. W., Investigation of the oxidation of hot-pressed Si_3N_4 with infra-red reflection spectroscopy (IRRS). *J. Mater. Sci.*, **16** (1981) 2767–73.
14. Raider, S. I., Flitsch, R., Aboaf, J. A. & Pliskin, W. A., Surface oxidation of silicon nitride films. *J. Electrochem. Soc.*, **123**(4) (1976) 506–15.
15. Deal, E. & Grove, A. S., General relationship for the thermal oxidation of silicon. *J. Appl. Phys.*, **36**(12) (1965) 3770–8.
16. Rigo, S., *Instabilities in Silicon Devices*. North-Holland, Amsterdam, 1986, pp. 32–62.
17. Crank, J., *The Mathematics of Diffusion*. Oxford University Press, 1975, pp. 266–85.
18. Schlichting, J., Oxygen transport through silica surface layers on silicon-containing ceramic materials. *J. High Temperatures—High Pressures*, **14**(6) (1982) 717–24.
19. Du, H., Tressler, R. E., Spear, K. & Pantano, C. G., Oxidation studies of crystalline CVD silicon nitride. *J. Electrochem. Soc.*, **136**(5) (1990) 1527–35.